

INTERPRETABLE MODELING OF ARTICULATORY TEMPORAL DYNAMICS FROM REAL-TIME MRI FOR PHONEME RECOGNITION

Jay Park^{1*}, Hong Nguyen^{1*}, Sean Foley^{1,2}, Jihwan Lee¹,
Yoonjeong Lee¹, Dani Byrd², Shrikanth Narayanan^{1,2}

¹Signal Analysis and Interpretation Lab, University of Southern California

²Department of Linguistics, University of Southern California

ABSTRACT

Real-time Magnetic Resonance Imaging (rtMRI) visualizes vocal tract action, offering a comprehensive window into speech articulation. However, its signals are high dimensional and noisy, hindering interpretation. We investigate compact representations of spatiotemporal articulatory dynamics for phoneme recognition from midsagittal vocal tract rtMRI videos. We compare three feature types: (1) raw video, (2) optical flow, and (3) six linguistically-relevant regions of interest (ROIs) for articulator movements. We evaluate models trained independently on each representation, as well as multi-feature combinations. Results show that multi-feature models consistently outperform single-feature baselines, with the lowest phoneme error rate (PER) of 0.34 obtained by combining ROI and raw video. Temporal fidelity experiments demonstrate a reliance on fine-grained articulatory dynamics, while ROI ablation studies reveal strong contributions from tongue and lips. Our findings highlight how rtMRI-derived features provide accuracy and interpretability, and establish strategies for leveraging articulatory data in speech processing. The source code is publicly available.¹

Index Terms— phoneme recognition, vocal tract regions of interest, real-time MRI, phoneme error rate

1. INTRODUCTION

Speech production is fundamentally articulatory; phonemes emerge from the coordination of constriction actions in the vocal tract. These actions, defined by constriction location and degree, involve articulators such as the lips, tongue, velum, and larynx [1]. Neural activity in the human sensorimotor cortex is highly correlated with these articulatory gestures [2], underscoring their central role in both cognitive and motor models of speech.

Capturing articulatory dynamics provides not only a scientific lens on human speech but also a powerful complement to acoustic-based processing. Articulatory data have

been obtained with instruments such as Electromagnetic Articulography (EMA) and ultrasound; however these capture only subsets of vocal tract variables —e.g., EMA lacks data tracking from the velum, tongue root, and larynx. Real-time magnetic resonance imaging (rtMRI) provides a fuller view of the vocal tract, including the posterior tongue root and laryngeal regions [3,4]. Midsagittal rtMRI has enabled applications such as vowel-consonant-vowel and phoneme sequence prediction [5, 6], speech-to-rtMRI synthesis [7], and rtMRI-to-speech synthesis [8]. However, unprocessed rtMRI video frames, while spatially rich, lack structured interpretable articulatory features and are high dimensional and noisy, complicating both training and interpretation.

While some studies have fed raw rtMRI frames directly into speech processing models in various applications, this approach suffers from high dimensionality and limited interpretability. Other articulator tracking modalities such as EMA, which has excellent temporal resolution but relies on limited point-tracking, have emphasized articulatory dynamics more explicitly and that success highlights the value of focusing on dynamics rather than static frames [9–11]. Recent work has shown a strong correlation between self-supervised acoustic representations and vocal tract dynamics [12], underscoring the centrality of articulatory motion in speech modeling. However, EMA provides only sparse sampling of the vocal tract and misses tongue root, velum and laryngeal action [13]. rtMRI, on the other hand, captures a full midsagittal view of the vocal tract but demands methods that can distill its high-dimensional frames into compact, interpretable representations.

Given these limitations, our study proposes effective preprocessing strategies for embedding articulatory motion in rtMRI videos for downstream tasks such as phoneme sequence prediction. We address two research questions: (1) How can speech-relevant information best be extracted from rtMRI video while balancing dimensionality and informativity? and (2) Which articulatory features are most critical for phoneme sequence prediction? To address these, we evaluate preprocessing methods that encode articulatory motion into low-dimensional yet informative representations. Such

¹https://github.com/usc-sail/multimodal_av_temporal_phoneme

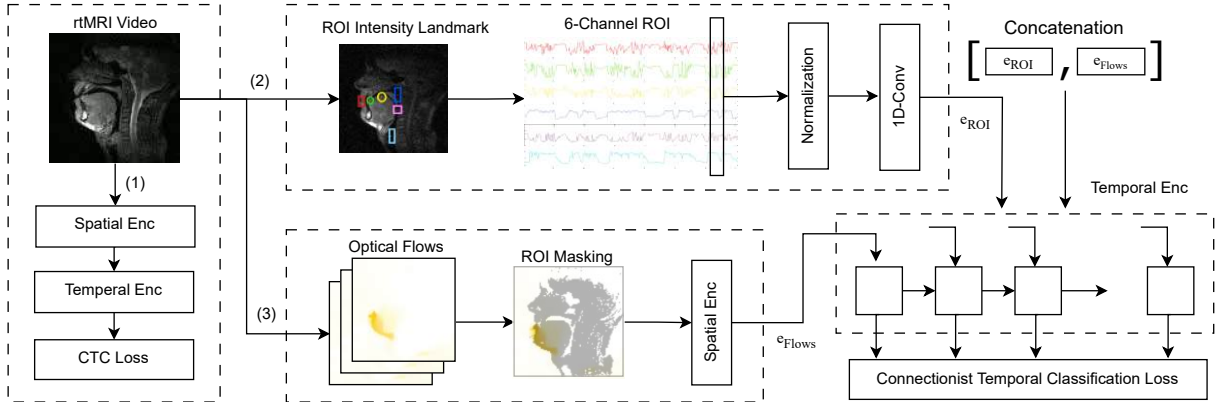


Fig. 1: Overview of three model pipelines for analyzing spatial–temporal articulatory dynamics in rtMRI. (1) Raw video frames, (2) Six-channel ROI pixel intensity, and (3) Optical flow encodes fine-grained articulatory kinematics.

representations can both improve recognition accuracy and enhance model interpretability, while reducing training complexity and risk of overfitting. Our contributions are:

- We evaluate optical flow and ROI intensity as representations of spatial and temporal information in rtMRI videos. While raw video alone yields the lowest phoneme error rate (PER) among single-feature models, combining feature types consistently outperforms single inputs.
- We show that phoneme sequence prediction from six-channel ROI features depends most strongly on lips, tongue tip and tongue root. Temporal fidelity tests of rtMRI features through shuffle, reversal, and resampling further demonstrate that accurate phoneme recognition relies on specific fine-grained articulatory dynamics.

Together, these findings demonstrate how targeted rtMRI preprocessing yields compact yet informative articulatory representations, advancing both interpretable speech modeling and efficient phoneme recognition.

2. METHODS

We examine spatial-temporal articulatory dynamics using two different methods: ROI pixel intensity maps and optical flow. Let the articulatory state at time t be $s_t \in \mathcal{S} \subset \mathbb{R}^{W \times H}$ (rtMRI domain). Observations are modality-specific mappings $h_m(s_t)$ in which h_{flows} and h_{ROI} are defined as optical flow representation and ROI pixel intensity, respectively. We hypothesize that h_{flows} captures high spatial resolution and directly encodes kinematics in rtMRI videos while h_{ROI} acts as a pooled, low-rank approximation of articulator dynamics robust to noise (averaging) but lacking fine-grained geometry. Finally, we provide experiments to verify these hypotheses.

2.1. Spatial-temporal dynamics via ROI Pixel Intensity

Using the VocalTract ROI Toolbox in MATLAB [14], we define six channels of regions of interest (ROIs) $\{\mathcal{R}_c\}_{c=1}^6 \subset \Omega$: lip aperture (LA), tongue tip (TT), tongue body (TB),

velum (VL), tongue root (TR), and larynx (LX). Regions were hand-selected by trained speech scientists based on pertinent vocal tract kinematics and spatial landmarks. Per-channel normalized intensity, as shown in Figure 1, is derived as $y_{t,c}^{\text{ROI}} = \frac{1}{|\mathcal{R}_c|} \int_{\mathcal{R}_c} \mathcal{I}_t(x) dx$. Therefore, the observation operator is a stacked normalized vector $h_{\text{ROI}}(s_t) = y_t^{\text{ROI}} = [y_{t,1}, y_{t,2}, \dots, y_{t,c}] \in \mathbb{R}^{t \times c}$, where t and c represent the temporal and spatial dimensions of the articulators, respectively. These features are processed with two layers of 1D convolution and a temporal encoder (LSTM/Mamba [15]) to generate articulatory embeddings. Finally, these embeddings are passed through a lightweight classification head to generate phoneme probability distributions (Figure 1).

2.2. Spatial-temporal dynamics via Optical Flow

Optical flow [16] is an alternative representation for modeling temporal dynamics in video sequences. Traditional optical flow methods [17] capture pixel-level motion but produce noisy representations at the object level, particularly in rtMRI video. While no deep learning models have been trained on medical images due to the lack of ground-truth annotations, our qualitative evaluation suggests that MemFlow [16], whose checkpoint was pretrained on the Sintel dataset [18], captures object-level motion patterns in rtMRI to some extent. Therefore, we extract optical flow fields $\mathcal{F}_t(x) \in \mathbb{R}^{t \times C \times W \times H}$ from video set v , where $C = 2$ represents horizontal and vertical motion components. To stabilize noise in the estimated optical flow, we suppress irrelevant background motion by applying a mask derived from intensity thresholding of the original images, thereby retaining only articulator-related movements. The masked flows are subsequently encoded with a Vision Transformer [19] to obtain spatial flow embeddings $e_{\text{flows}} \in \mathbb{R}^{T \times D}$. Temporal dependencies are then modeled using a temporal encoder (Mamba/LSTM), and the output embeddings are passed through a lightweight classification head to generate phoneme probability distributions in a way identical to the ROI approach (Figure 1).

Table 1: PER of comparison models from [6] (top), PER from uni-feature models in current study (middle), and PER from multi-feature models in current study (bottom). The best scores for each metric are in bold. DIV: Training Divergence, N/A: Not reported, ✱: Frozen weights.

| rtMRI Features | Spatial Enc | Temp Enc | PER↓ | Phone Acc↑ Top-1 Top-3 |
|--------------------------------|-------------|------------------|-------------|---------------------------|
| <i>Results reported by [6]</i> | | | | |
| Raw Video | ViT-B ✱ | LSTM + Conformer | 0.49 | N/A |
| <i>Uni-Feature</i> | | | | |
| Raw Video | | Mamba | DIV | - |
| | ResNet | Mamba | 0.37 | 11.7 67.6 |
| | ResNet | LSTM | 0.38 | 12.8 67.7 |
| Flows | ResNet | Mamba | 0.41 | 11.2 67.5 |
| | ResNet | LSTM | 0.43 | 8.6 44.4 |
| 6C-ROI | Conv1D | LSTM | 0.53 | 12.2 49.9 |
| | Conv1D | Mamba | 0.61 | 9.2 48.9 |
| <i>Multi-Feature</i> | | | | |
| 6C-ROI + Flows | | | 0.35 | 15.1 66.5 |
| 6C-ROI + Raw Video | | | 0.34 | 14.8 64.1 |
| Raw Video + Flows | | | 0.39 | 15.3 66.4 |

3. EXPERIMENTAL SETUP

3.1. Dataset

We utilize an rtMRI audio/video dataset of one male American English speaker presented in [20]. Speech in this dataset, the "longest single speaker" corpus available to date, contains the 460 phrases from the USC TIMIT [21] corpus, the phrases from the USC 75-Speaker Dataset [22], and spontaneous response to questions about daily activities. This dataset consists of approximately one hour of speech recorded using a midsagittal orientation of the vocal tract with a 0.55T MRI scanner and a custom receiver coil for the upper airway [23]. The dataset consists of 71 videos with a frame rate of 99 frames/sec (FPS) [24], audio with a sampling rate of 16 kHz, and phoneme-level annotations.

3.2. Preprocessing

Videos were resampled to 100 FPS to simplify preprocessing. Audio and video sequences were sliced into 5 second samples with a 2.5 second sliding window, resulting in 1224 samples and a total duration of 102 minutes. 924 samples from videos 18-71 were used for training, 100 samples from videos 13-17 were used for validation, and 100 samples from videos 1-12 were used for testing. Video samples $\mathbf{V} \in \mathbb{R}^{500 \times 104 \times 104}$ were then converted to optical flow and ROI representations.

3.3. Training

For phoneme sequence prediction on running speech, we use the Connectionist Temporal Classification (CTC) loss func-

Table 2: PER increase from temporal fidelity tests. Features with the highest increase in PER for each test type are in bold.

| rtMRI Features | Cross-Phon. | Per-Phon. | Time-Rev. | Up Samp. | Down Samp. |
|----------------|-------------|-------------|-------------|-------------|-------------|
| Raw Vid. | 0.28 | 0.21 | 0.25 | 0.30 | 0.20 |
| Flows | 0.48 | 0.04 | 0.07 | 0.22 | 0.24 |
| 6C-ROI | 0.07 | 0.15 | 0.12 | 0.02 | 0.03 |

Table 3: PER increase of five-channel ROI model upon removing articulatory features. Largest changes are in bold.

| LA | TT | TD | VL | TR | LX |
|------|-------------|------|------|------|------|
| 0.13 | 0.15 | 0.10 | 0.03 | 0.06 | 0.08 |

tion [25] to train all of our models. Utilizing an NVIDIA A40 GPU, we train with a batch size of 1 and an Adam optimizer with an initial learning rate of 10^{-3} and a weight decay of 10^{-4} to regularize parameters. The learning rate was scheduled to decay by a factor of 0.9 every 20 epochs over 300 total epochs using a step scheduler. While [6] compared PER for models trained on audio, raw video, and both combined, we measure performance of models trained independently on raw video, optical flow and vocal tract ROI, as well as for models combining pairs of these features.

3.4. Evaluation metrics

We evaluate model performance using two metrics: sequence-level PER and per-phoneme classification accuracy (Top-1 and Top-3) on the test set. For each phoneme y_i , we calculate Top-1 and Top-3 per-phoneme classification accuracy $\mathbf{P}_{\text{Acc}} = \frac{\# \text{correct frames for } y_i}{\text{Total frames for } y_i}$ to show which phonemes are problematic (e.g., the model struggles with /d/, but not with /s/). Confusion matrices show the associated substitution patterns (e.g., /p/ and /b/, /s/ and /f/).

4. RESULTS AND DISCUSSION

4.1. Comparison of features

PER and per-phoneme classification accuracy (Top-1 and Top-3) for each speech representation are shown in Table 1. Since [6] predicted phoneme sequences with the same rtMRI corpus, we include their results for comparison although our testing dataset is different. Models trained independently on raw video, optical flow, and six-channel ROI have the best PER values of 0.37, 0.41, and 0.53 respectively. While Top-1 per-phoneme classification accuracy remains consistent for all features, Top-3 per-phoneme classification accuracy is best with raw video and optical flow models.

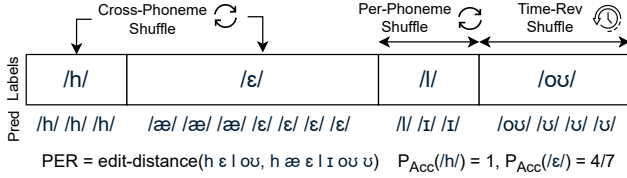


Fig. 2: Shuffle tests for temporal fidelity evaluation with example of PER and P-Acc calculation.

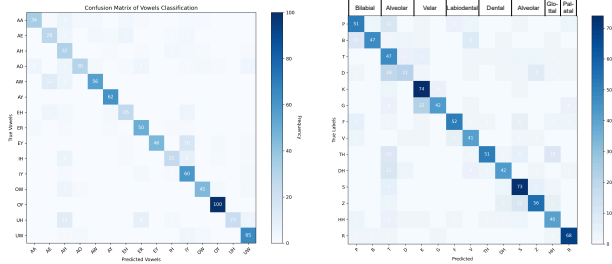


Fig. 3: Confusion matrices in percentage of 6-Channel ROI + raw video showing vowels (left) and consonants (right). We ignore the Palatal Consonants /SH/ and /ZH/ since sample size for each is low.

The results for PER and per-phoneme classification accuracy of multimodal models trained on pairs of rtMRI-acquired features are also presented in Table 1. We also present confusion matrices for our best-performing model trained on six-channel ROI and raw video in Figure 3. These matrices show that most phonemes are recognized to varying degrees apart from /ʒ/ and /ʃ/. The matrices also show errors between similar consonants (e.g., velars /k/ and /g/). While Top-3 per-phoneme classification accuracy fails to exceed that of single feature models, Top-1 per-phoneme classification accuracy is improved by using multiple features. The lowest PER of 0.34 was acquired with a multimodal model trained on six-channel ROI and raw video, indicating that these two feature types provide complementary information.

4.2. Temporal fidelity

We investigate the role of temporal dynamics in rtMRI by rearranging frames using five methods (Figure 2):

- 1. Cross-phoneme shuffle:** Phoneme order is shuffled while frame order within each phoneme is maintained. This approach tests the relevance of phoneme order.
- 2. Per-phoneme shuffle:** Frame order is shuffled within each phoneme while phoneme order is maintained to test the relevance of temporal dynamics within each phoneme.
- 3. Time-reversal:** The order of frames is reversed in sequence within each phoneme. This approach preserves smoothness while flipping direction of motion. This approach tests sensitivity to causal dynamics.

- 4. Upsampling:** Frames are upsampled by a factor of two.
- 5. Downsampling:** Frames are downsampled by a factor of two to test sensitivity to temporal resolution.

We present results for our temporal fidelity analysis in Table 2. The increase in PER with models retrained on shuffled data for all video features suggests that embeddings rely heavily on temporal continuity and cues from coarticulation. The PER increases of 0.20, 0.24, and 0.03 upon downsampling raw video, Optical Flow, and ROI respectively demonstrate sensitivity to high frequency components. Meanwhile, the PER increases of 0.30, 0.22, and 0.02 upon upsampling raw video, Optical Flow, and ROI respectively may be attributed to model overfitting with a larger number of parameters.

4.3. Ablation: Importance of each ROI

We explore which articulators play a more critical role in capturing articulatory motion. Adopting a similar methodology to [26], we train a model with each ROI removed and then calculate the PER difference compared to the full model. The PER increases after removing each channel are shown in Table 3. The largest changes occur when removing TT and LA regions, with PER increases of 0.13 and 0.15 respectively. This implies that articulators are complementary, with especially strong contributions from the information associated with tongue tip constriction and bilabial action.

5. CONCLUSION AND FUTURE WORK

Our study shows that rtMRI preprocessing choices strongly shape both accuracy and interpretability in phoneme recognition. Multi-feature models (e.g., ROI + raw video) consistently outperform single inputs: ROI features provide compact, interpretable summaries, while raw video and optical flow preserve richer kinematic detail. Confusion analyses highlight errors in phonetically similar categories, temporal fidelity tests confirm reliance on within-phoneme dynamics, and ablations reveal the central role of lip and tongue movements. Together, these findings underscore the complementarity of feature types, with combined representations offering both efficiency and performance.

As a last note, given that manual ROI extraction is time consuming, future work can seek to automate ROI feature extraction using technically optimal strategies. A key limitation of our work is our reliance on one subject, restricting cross-subject generalization and lessening the need for cross-subject video and region normalization for different vocal tracts. Consequently, our models may overfit to individual articulators. The dataset also lacks certain phonemes (/ʒ/ in particular), thereby increasing PER. Future studies should expand to multi-subject datasets with phoneme-aligned labels and vocal-tract normalization for constriction location and degree to improve generalizability.

6. ACKNOWLEDGEMENT

This work was supported by The U.S. National Science Foundation under Grant NSF (IIS-2311676, BCS-2240349, RI-2106930). We would like to thank Prof. Sudarsana Reddy Kadiri for his valuable comments and insights.

7. REFERENCES

- [1] Catherine P Browman and Louis Goldstein, “Articulatory phonology: An overview,” *Phonetica*, vol. 49, no. 3-4, pp. 155–180, 1992.
- [2] Josh Chartier et al., “Encoding of articulatory kinematic trajectories in human speech sensorimotor cortex,” *Neuron*, vol. 98, no. 5, pp. 1042–1054.e4, 2018.
- [3] Shrikanth S. Narayanan, Krishna S. Nayak, Sungbok Lee, Abhinav Sethy, and Dani Byrd, “An approach to real-time magnetic resonance imaging for speech production,” *Journal of the Acoustical Society of America*, vol. 115, pp. 1771–1776, 2004.
- [4] Sajan G Lingala, Yinghua Zhu, Yoon-Chul Kim, Asterios Toutios, Shrikanth S. Narayanan, and Krishna S. Nayak, “A fast and flexible mri system for the study of dynamic vocal tract shaping,” *Magnetic Resonance in Medicine*, 2016.
- [5] Pramit Saha et al., “Towards automatic speech identification from vocal tract shape dynamics in real-time mri,” in *Interspeech 2018*, 2018, pp. 1249–1253.
- [6] Sean Foley, Hong Nguyen, Jihwan Lee, Sudarsana Reddy Kadiri, Dani Byrd, Louis Goldstein, and Shrikanth Narayanan, “Towards disentangling the contributions of articulation and acoustics in multimodal phoneme recognition,” *arXiv preprint arXiv:2505.24059*, 2025.
- [7] Hong Nguyen, Sean Foley, Kevin Huang, Xuan Shi, Tiantian Feng, and Shrikanth Narayanan, “Speech2rtmri: Speech-guided diffusion model for real-time mri video of the vocal tract during speech,” in *ICASSP 2025 - 2025 IEEE International Conference on Acoustics, Speech and Signal Processing (ICASSP)*, 2025, pp. 1–5.
- [8] Neil Shah, Ayan Kashyap, Shirish Karande, and Vineet Gandhi, “Mri2speech: Speech synthesis from articulatory movements recorded by real-time mri,” in *ICASSP 2025-2025 IEEE International Conference on Acoustics, Speech and Signal Processing (ICASSP)*. IEEE, 2025, pp. 1–5.
- [9] Asterios Toutios, Slim Ouni, and Yves Laprie, “Estimating the control parameters of an articulatory model from electromagnetic articulograph data,” *The Journal of the Acoustical Society of America*, vol. 129 5, pp. 3245–57, 2011.
- [10] Asterios Toutios and Shrikanth S. Narayanan, “Articulatory synthesis of french connected speech from ema data,” in *Interspeech*, 2013.
- [11] Dani Byrd and Elliot Saltzman, “Intragesural dynamics of multiple prosodic boundaries,” *Journal of Phonetics*, vol. 26, no. 2, pp. 173–199, 1998.
- [12] Cheol Jun Cho et al., “Evidence of vocal tract articulation in self-supervised learning of speech,” in *ICASSP 2023 - 2023 IEEE International Conference on Acoustics, Speech and Signal Processing (ICASSP)*, 2023, pp. 1–5.
- [13] Asterios Toutios and Shrikanth S. Narayanan, “Advances in real-time magnetic resonance imaging of the vocal tract for speech science and technology research,” *APSIPA Transactions on Signal and Information Processing*, vol. 5, 2016.
- [14] R. Blaylock, “reedblaylock/vocaltract-roi-toolbox,” July 2021.
- [15] Albert Gu and Tri Dao, “Mamba: Linear-time sequence modeling with selective state spaces,” *arXiv preprint arXiv:2312.00752*, 2023.
- [16] Qiaole Dong and Yanwei Fu, “Memflow: Optical flow estimation and prediction with memory,” in *2024 IEEE/CVF Conference on Computer Vision and Pattern Recognition (CVPR)*, 2024, pp. 19068–19078.
- [17] Bruce D. Lucas and Takeo Kanade, “An iterative image registration technique with an application to stereo vision,” in *International Joint Conference on Artificial Intelligence*, 1981.
- [18] Daniel J. Butler, Jonas Wulff, Garrett B. Stanley, and Michael J. Black, “A naturalistic open source movie for optical flow evaluation,” in *Proceedings of the 12th European Conference on Computer Vision - Volume Part VI*, Berlin, Heidelberg, 2012, ECCV’12, p. 611–625, Springer-Verlag.
- [19] Ashish Vaswani, Noam Shazeer, Niki Parmar, Jakob Uszkoreit, Llion Jones, Aidan N. Gomez, Lukasz Kaiser, and Illia Polosukhin, “Attention is all you need,” in *Proceedings of the 31st International Conference on Neural Information Processing Systems*, Red Hook, NY, USA, 2017, NIPS’17, p. 6000–6010, Curran Associates Inc.
- [20] Sean Foley, Jihwan Lee, Kevin Huang, Xuan Shi, Yoonjeong Lee, Louis Goldstein, and Shrikanth Narayanan, “A long-form single-speaker real-time mri speech dataset,” in *ICASSP 2026 - 2026 IEEE International Conference on Acoustics, Speech and Signal Processing (ICASSP)*, 2026, pp. 1–5.
- [21] Shrikanth S. Narayanan et al., “Usc-timit : A database of multimodal speech production data,” *J. Acoust. Soc. Am.*, vol. 136, no. 3, pp. 1307–1311, sep 2014.
- [22] Yongwan Lim et al., “A multispeaker dataset of raw and reconstructed speech production real-time mri video and 3d volumetric images,” *Scientific data*, vol. 8, no. 1, pp. 187, 2021.
- [23] Felix Muñoz et al., “Evaluation of a novel 8-channel rx coil for speech production mri at 0.55 t,” *Magnetic Resonance Materials in Physics, Biology and Medicine*, vol. 36, pp. 419–426, 2022.
- [24] Prakash Kumar et al., “State-of-the-art speech production mri protocol for new 0.55 tesla scanners,” *Interspeech 2024*, 2024.
- [25] Alex Graves, Santiago Fernández, Faustino Gomez, and Jürgen Schmidhuber, “Connectionist temporal classification: labelling unsegmented sequence data with recurrent neural networks,” in *Proceedings of the 23rd International Conference on Machine Learning*, New York, NY, USA, 2006, ICML’06, p. 369–376, Association for Computing Machinery.
- [26] Jihwan Lee, Kevin Huang, Kleanthis Avramidis, Simon Pistrosch, Monica Gonzalez-Machorro, Yoonjeong Lee, Björn W. Schuller, Louis Goldstein, and Shrikanth Narayanan, “Articulatory Feature Prediction from Surface EMG during Speech Production,” in *Interspeech 2025*, 2025, pp. 320–324.